Separation and Purification Technology 278 (2022) 119495

Contents lists available at ScienceDirect

Separation and Purification Technology

journal homepage: www.elsevier.com/locate/seppur

Preparation of new triptycene- and pentiptycene-based crosslinked polymers and their adsorption behavior towards aqueous dyes and phenolic organic pollutants

Shiyuan Zhou [a], Peiyang Gu [a], Haibo Wan [a], Yutao Zhu [a], Najun Li [a], Dongyun Chen [a], Antonio Marcomini [b], Qingfeng Xu [a,*], Jianmei Lu [a,*]

[a] College of Chemistry, Chemical Engineering and Materials Science, Collaborative Innovation Center of Suzhou Nano Science and Technology, Soochow University, Suzhou, Jiangsu 215123, China

[b] Department of Environmental Sciences, Informatics and Statistics, University Ca' Foscari Venice, I-30170 Venice, Italy

ARTICLE INFO

Keywords:
Triptycene-based crosslinked polymers
Adsorption
Phenolic organic pollutants

ABSTRACT

Rigid triptycene- and pentiptycene-based monomers, with intrinsic hierarchical structures, were polymerized using tetrafluoroterephthalonitrile as the crosslinker to fabricate crosslinked porous architectures named P1 and P2. The reaction is simple and can be conducted at a relatively mild temperature. Both P1 and P2 exhibit good thermal stability, and good adsorption performance for dyes and phenolic organic pollutants including MB, MO, Pol and BPA. The removal efficiency of P2 is >99% within 10 min for BPA and an adsorption equilibrium for Pol can be reached within 5 min. The adsorption kinetics fit the pseudo-second-order model and the adsorption isotherms follow the Langmuir model and the maximum adsorption capacity of P1 and P2 for BPA can reach 212.06 mg g^{-1} and 330.02 mg g^{-1}, respectively. In addition, the obtained crosslinked polymers show a highly selective adsorption capacity towards phenolic organic pollutants. Featuring a simple synthesis, porous architecture and efficient adsorption capability, such triptycene-based and pentiptycene-based crosslinked polymers may be ideal adsorbents for water treatment and purification.

1. Introduction

In the past few decades, the rapid development of industry has caused serious environmental pollution, resulting in water contamination and lack of clean water; this threatens the daily life and health of millions of people [1]. Persistent organic pollutants (POPs) including organic raw materials, dyes, pharmaceuticals, and phenolic pollutants are mainly derived from industrial waste and are the main problems associated with drinking water safety[2,3]. Owing to their biotoxicity, mutagenicity, carcinogenicity and oncogenicity, POPs dramatically increase the probability of suffering from various unexpected diseases but they are hard to effectively remove under natural conditions due to their high stability[1,4–6]. Especially bisphenol A (BPA), as representative phenolic organic pollutants and one of the most broadly used raw materials to prepare epoxy resins and polycarbonate plastics, has been reported to have been widely spread in the sea, groundwater, even drinking water owing to the indiscriminate discharge of industrial waste water[7,8]. The main harm of BPA to human body are reflected in biotoxicity and carcinogenicity, probably leading to endocrine dyscrasia [9,10].

Therefore, the development of approaches to achieve efficient removal of POPs are of great importance. Currently, essential approaches to remove POPs include adsorption, photocatalysis, biodegradation, and membrane filtration, etc. [11–21].Among these methods, adsorption with high efficiency, low cost, simplicity and convenience have been widely adopted and studied.[22–28]

The adsorbent is the key part of the adsorption process. Crosslinked polymers have attracted significant attention owing to their stable structure, designability, diversity, low density, and highly efficient adsorption, [29–33]. One of the current synthetic strategies for the preparation of crosslinked polymers involves the selection of functional monomers with intrinsic pores or specific properties which can be polymerized with suitable connecting molecules to give highly crosslinked porous structures[34–37]. Due to the simplicity, designability and tunable porosity, this synthetic strategy is still the most commonly used at present [38–40]. Triptycene and its derivatives with rigid and

* Corresponding authors.
E-mail addresses: xuqingfeng@suda.edu.cn (Q. Xu), lujm@suda.edu.cn (J. Lu).

https://doi.org/10.1016/j.seppur.2021.119495
Received 28 June 2021; Received in revised form 10 August 2021; Accepted 13 August 2021
Available online 16 August 2021

hierarchical structures have been widely reported as functional monomers to prepare crosslinked polymers for adsorption applications [41,42]. Xu and coworkers[43] developed a one-pot Friedel-Crafts alkylation polymerization of triptycenes using formaldehyde dimethyl acetal as a cross-linker and synthesized a triptycene-based crosslinked polymer with excellent capacity for dye adsorption. Additionally, Das and coworkers[44] used a Cu(I) catalyzed azide-alkyne Click reaction to synthesize a triptycene-based and 1,2,3-triazole crosslinked polymer with high CO_2 capture capability and organic dye adsorption. However, as far as we know, the use of triptycene-based or pentiptycene-based crosslinked polymers with applications in the adsorption of phenolic organic pollutants, especially BPA are quite rare.

Herein, we synthesized two triptycene- and pentiptycene-based crosslinked polymers, P1 and P2, respectively, using tetrafluoroterephthalonitrile (TFTP) as the crosslinker. (Scheme 1) The polymerization reaction occurred at a relatively mild temperature under the catalysis of 1,5-diazabicyclo(5,4,0)undec-5-ene (DBU). The synthesized pentiptycene-based polymers were characterized in terms of chemical structure, thermal properties and their adsorption performance with regards to dyes and phenolic organic pollutants at low concentration. The twisted triptycene-based monomers crosslinked by a representative crosslinker contribute to the construction of a porous skeleton for both P1 and P2, endowing rapid and efficient adsorption capacity for phenolic organic pollutants such as phenol and bisphenol A at low concentration in aqueous solution. Additionally, the adsorption performance of both P1 and P2 for non-hydroxyl aromatic organic pollutants and common alcohols was also investigated to evaluate their potential as materials for the selective adsorption of phenolic organic pollutants.

2. Experimental

2.1. Materials

All materials were purchased from TCI (Shanghai) Development Co. Ltd and all reagents were obtained from Sinopharm Chemical Reagent Co. Ltd and used as received, without further purification, unless otherwise stated. All chemical reagents and solvents were used without further purification.

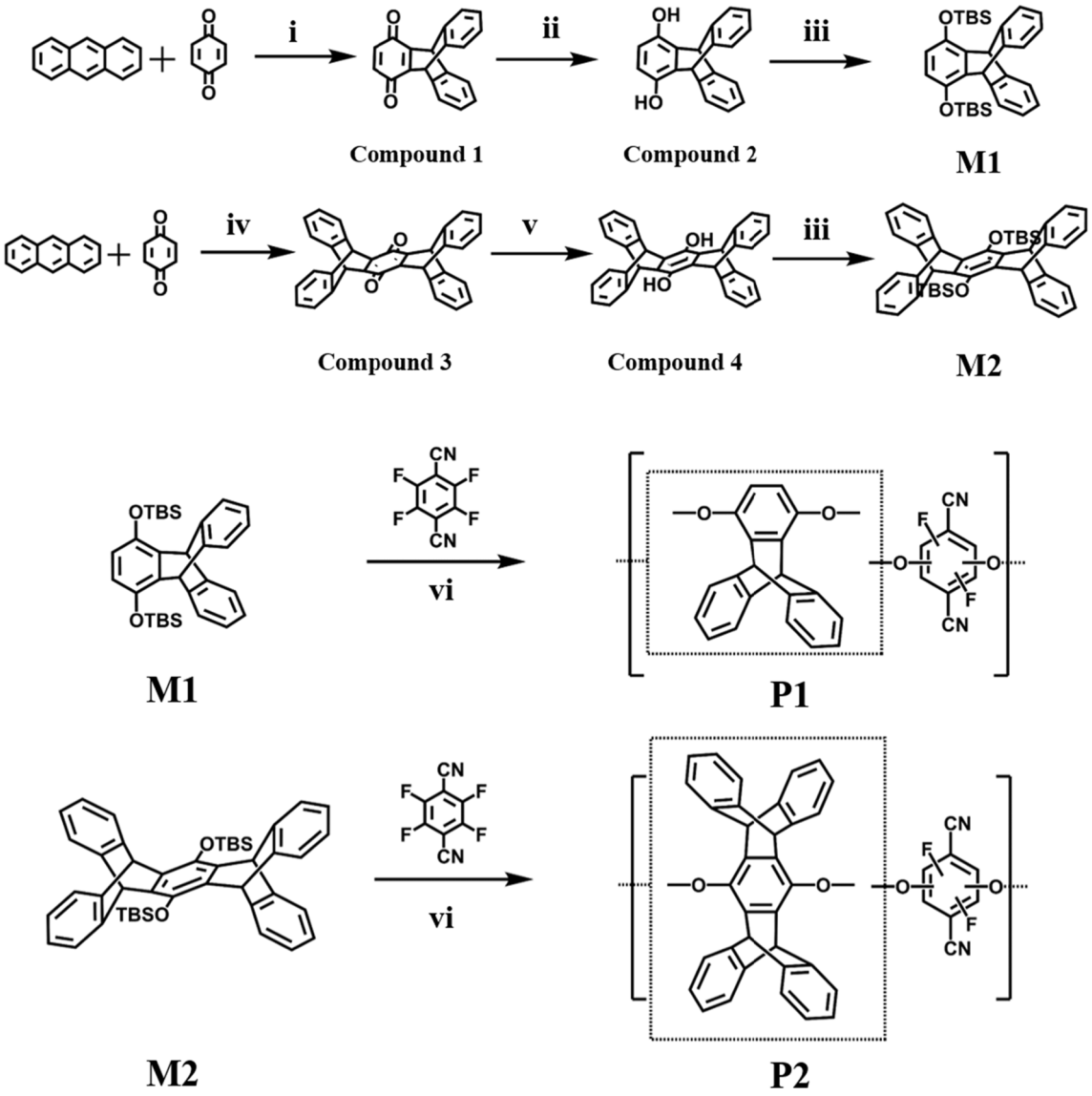

Scheme 1. Synthetic procedure towards crosslinked polymers termed P1 and P2. i: Xylene; ii: KOH, CH_3CH_2OH; iii: TBSCl; iv: Chloranil, CH_3COOH; v: $NaBH_4$, CH_3OH; vi: DBU, DMF.

2.2. Synthetic procedure

2.2.1. Synthesis of (9r,10r)-9,10-dihydro-9,10-[1,2]benzenoanthracene-13,16-dione (Compound 1)

Anthracene (7.1 g, 40 mmol) and 1,4-benzoquinone (4.39 g, 40 mmol) were dissolved in xylene (50 mL) under an argon atmosphere, then the reaction mixture was stirred and heated at reflux for 3 h. After the reaction was complete, the mixture was cooled to room temperature. Then the mixture was filtered, washed with ethanol and dried at 60 °C under vacuum to obtain 10.4 g light yellow product with a yield of 91%. The product was directly used in the next reaction procedure without further characterization.

2.2.2. Synthesis of (9r,10r)-9,10-dihydro-9,10-[1,2]benzenoanthracene-1,4-diol (Compound 2)

Compound 1 (8.52 g, 30 mmol) was dissolved in glacial acetic acid (70 mL) in a 250 mL flask under an argon atmosphere. A few drops of hydrobromic acid (40%) were added and the mixture was heated to reflux for 2 h. After the reaction was complete, the mixture was cooled to room temperature. A white powder (7.95 g) was obtained by filtration with a yield of 93%. The product was directly used in the next reaction procedure without further characterization.

2.2.3. Synthesis of (9r,10r)-1,4-bis((tert-butyldimethylsilyl)oxy)- 9,10-dihydro-9,10-[1,2]benzenoanthracene (M1)

Compound 2 (2.86 g, 10 mmol) and imidazole (1.7 g, 25 mmol) were dissolved in dichloromethane (40 mL) in a 250 mL flask. Tert-butyldimethylsilyl chloride (3.75 g, 25 mmol) was dissolved in 10 mL dichloromethane and then added dropwise to the above mixture. The reaction was stirred at room temperature overnight and monitored by thin layer chromatography (TLC). After the reaction was complete, the mixture was filtered and the filtrate was concentrated by rotary evaporation. The crude product was purified by silica-gel column chromatography with a mixture of dichloromethane and petroleum ether (1/5, v/v) to give a white powder (4.4 g) with a yield of 86%. ^{1}H NMR (400 MHz, DMSO-d_6, ppm) δ 7.38 (s, 2H), 7.00 (s, 2H), 6.43 (s, 1H), 5.72 (s, 1H), 1.10 (s, 9H), 0.17 (s, 6H). ^{13}C NMR (101 MHz, $CDCl_3$) δ 144.61, 143.44, 135.49, 123.82, 122.66, 115.36, 47.09, 24.86, 17.27. HRMS: calc. Mass: *m/z* 514.2723, found 514.2720.

2.2.4. Synthesis of (5r,7r,12r,14r)-5,7,12,14-tetrahydro- 5,14:7,12-bis ([1,2]benzeno)pentacene-6,13-dione (Compound 3)

Anthracene (7.1 g, 40 mmol), chloranil (9.8 g, 40 mmol) and 1,4-benzoquinone (2.6 g, 24 mmol) were dissolved with glacial acetic acid (200 mL) in a 500 mL flask under an argon atmosphere. The mixture was heated at reflux for 16 h and monitored by TLC. After the reaction was complete, the mixture was cooled to room temperature and then filtered. The solid was washed with anhydrous ether and ethanol continuously, and dried at 60 °C under vacuum to give 8.1 g of a yellow powder with a yield of 88%. The product was directly used in the next reaction procedure without further characterization.

2.2.5. Synthesis of (5r,7r,12r,14r)-5,7,12,14-tetrahydro- 5,14:7,12-bis ([1,2]benzeno)pentacene-6,13-diol (Compound 4)

Compound 3 (6.9 g, 15 mmol) and sodium borohydride (1.14 g, 30 mmol) were dissolved in anhydrous tetrahydrofuran (60 mL) in a 100 mL two-necked flask under an argon atmosphere. Then, 30 mL anhydrous methanol was added dropwise into the mixture and the reaction was stirred at room temperature for 1 h. After the reaction was completed, the mixture was filtered and dried under vacuum at 60 °C to give 6.2 g of a white powder with a yield of 89%. The product was directly used in the next reaction procedure without further characterization.

2.2.6. Synthesis of (5r,7r,12r,14r)-6,13-bis((tert-butyldimethylsilyl)oxy)-5,7,12,14-tetrahydro-5,14:7,12-bis([1,2]benzeno)pentacene (M2)

Compound 5 (4.62 g, 10 mmol) and imidazole (1.7 g, 25 mmol) were dissolved with 60 mL THF in a 250 mL flask. Tert-butyldimethylsilyl chloride (3.75 g, 25 mmol) was dissolved in 10 mL THF and then added dropwise to the mixture. The reaction was stirred at room temperature overnight and monitored by TLC. After the reaction was complete, the mixture was filtered and the filtrate was concentrated by rotary evaporation. The crude product was purified via silica-gel column chromatography with a mixture of dichloromethane and petroleum ether (1/3, v/v) to give a white powder (5.7 g) with a yield of 83%. ^{1}H NMR (400 MHz, $CDCl_3$, ppm) δ 7.27 – 7.24 (m, 8H), 6.96 – 6.84 (m, 8H), 5.63 (s, 4H), 1.31 (s, 18H), 0.42 (s, 12H). ^{13}C NMR (101 MHz, $CDCl_3$) δ 144.61, 143.44, 135.49, 123.82, 122.66, 115.36, 47.09, 24.86, 17.27. HRMS: calc. Mass: *m/z* 690.3349, found 690.3350.

2.2.7. Synthesis of P1

Compound 3 (0.515 g, 1 mmol) and tetrafluoroterephthalonitrile (0.2 g, 1 mmol) were added into a 50 mL Schlenk tube under an argon atmosphere. The tube was purged three times with argon and then charged with 5 mL DMF. The mixture was heated to 90 °C with stirring until the solid was completely dissolved and then 1,8-diazabicyclo [5.4.0]undec-7-ene (DBU, 30 μL, 0.2 mmol) was added dropwise to the reaction mixture. The reaction was stirred for 72 h and a red precipitate appeared. The mixture was poured into 200 mL anhydrous methanol with vigorous stirring and filtered. The obtained red precipitate was Soxhlet extracted with THF for 24 h and the residue was dried at 60 °C under vacuum. A scarlet-colored product (0.5 g) was obtained with a yield of 70%.

2.2.8. Synthesis of P2

Compound 6 (0.691 g, 1 mmol) and tetrafluoroterephthalonitrile (0.2 g, 1 mmol) were added into a 50 mL Schlenk tube under an argon atmosphere. The tube was purged three times with argon and then charged with 5 mL DMF. The mixture was heated to 90 °C with stirring until the solid was completely dissolved and then DBU (30 μL, 0.2 mmol) was added dropwised to the reaction mixture. The reaction was stirred for 72 h and a red precipitate appeared. The mixture was poured into 200 mL anhydrous methanol with vigorous stirring and filtered. The obtained red precipitate was Soxhlet extracted with THF for 24 h and the residue was heated at 60 °C under vacuum. A scarlet-colored product (0.55 g) was obtained with a yield of 62%.

2.2.9. Preparation of chromogenic reagent for phenolic organic pollutants

Reagent 1: 20 g ammonium chloride was dissolved in 100 mL ammonium hydroxide in a 100 mL brown volumetric flask. **Reagent 2**: 2 g 4-aminoantipyrine was dissolved in 100 mL distilled water in a 100 mL brown volumetric flask. **Reagent 3**: 8 g potassium ferricyanide was dissolved in 100 mL distilled water in a 100 mL brown volumetric flask. All the above reagents were sonicated to make sure the solutes were completely dissolved and then stored at 2 °C. When needed, a 3 mL solution containing phenolic organic pollutants was collected in a 5 mL vial, then 10 μL reagent 1, 20 μL reagent 2 and 20 μL reagent 3 were added successively. The obtained solution was vigorously shaken and immediately tested using a UV–vis spectrometer.

2.3Adsorption experiments

The adsorption capacity (q_e, mg g^{-1}) is calculated through the difference between the initial and final concentrations according to the following equation:

$$q_e = \frac{C_i - C_e}{m} V$$

where C_i and C_e (mg L^{-1}) are the initial and final concentrations, m (g) is the weight of the crosslinked polymers used in the adsorption experiments, and V (L) is the volume of the solutions of dyes or phenolic

organic pollutants.

Two mainly used models including the Freundlich model and the Langmuir model were adopted to investigate the maximum adsorption capacities of both P1 and P2.

The Freundlich model is:

$$\ln q_e = lnK_F + \frac{1}{n} lnC_e$$

The Langmuir model is:

$$\frac{C_e}{q_e} = \frac{C_e}{q_m} + \frac{1}{K_L q_m}$$

where q_e (mg g^{-1}) is the adsorption capacity in equilibrium; K_F and K_L are the constants of Freundlich and Langmuir models, respectively; $\frac{1}{n}$ is an empirical parameter of the Freundlich model; C_e (mg g^{-1}) is the concentrations of dyes or phenolic organic pollutants in equilibrium; q_m (mg g^{-1}) is the maximum adsorption capacity under ideal conditions.

The adsorption kinetics were analyzed by pseudo-first-order and pseudo-second-order kinetic models.

The pseudo-first-order kinetic model is:

$$\ln(q_e - q_t) = \ln q_e - k_1 t$$

And the pseudo-second-order kinetic model is:

$$\frac{t}{q_t} = \frac{1}{k_2 q_e^2} + \frac{t}{q_e}$$

where q_e (mg g^{-1}) is the adsorption capacity in equilibrium; q_t (mg g^{-1}) is the adsorption capacity in t (min); k_1 (min^{-1}) and k_2 (g mg^{-1} min^{-1}) are the constants of pseudo-first-order and pseudo-second-order models, respectively.

2.3. Characterization

^{1}H NMR spectra were recorded using INOVA-400 NMR spectrometers, with DMSO-d_6 and $CDCl_3$ as the solvent and tetramethylsilane (TMS) as the internal standard at ambient temperature. Solid-state ^{13}C NMR spectra were recorded on a Bruker INOVA-400 NMR spectrometer at ambient temperature. Mass spectra were performed with a GCT Premier high-resolution time-of-flight mass spectrometer and using EI as the ion source. Power X-ray diffraction (PXRD) of the crosslinking polymers was measured on an X'Pert-Pro MPD to analyze the crystallographic structure of the adsorbent materials. Fourier transform infrared (FT-IR) spectra were tested on a Nicolet-4700 spectrometer. Thermo-gravimetric Analysis (TGA) were carried out on a TA dynamic TGA 2960 instrument, rising from 25 °C to 800 °C with a N_2 flow rate of 50 mL min^{-1} at a heating rate of 10 °C min^{-1}. X-ray photoelectron spectroscopy of the adsorbent materials was carried out on an X-ray photoelectron spectrometer (XPS, ESCALAB MK II). The binding energies were calibrated by using adventitious carbon contamination (C (1 s) = 284.8 eV) as a charge reference. Scanning electron microscopy (SEM, Hitachi S-4700) together with SEM mapping, and transmission electron microscopy (TEM, Hitachi H600, 200 kV) were employed to observe the morphology, pore sizes, elemental distribution and content of the crosslinking polymers. The UV–vis spectra were tested using a CARY 50 spectrometer equipped with integrating sphere.

3. Results and discussion

3.1. Characterization of M1, M2, P1 and P2

The structures of M1 and M2 were characterized by ^{1}H NMR, ^{13}C NMR, high-resolution and Fourier transform infrared (FT-IR) spectroscopy and the results are shown in **Figs. S1–S7**. In addition, the structures of the crosslinked polymers P1 and P2 were characterized by FT-IR, solid-state ^{13}C NMR spectroscopy and TGA, XRD, SEM, and TEM analysis; the results are displayed in Figs. 1 and 2 and **Figs. S7–S10**. Firstly, P1 and P2 were analyzed via FT-IR to confirm their structures (Fig. 1**a**). The adsorption bands in the region of 1340–1510 cm^{-1} could be attributed to the stretching vibrations of the benzene rings. The peaks at 1202 cm^{-1} for P1, and 1213 cm^{-1} for P2, can be assigned to the stretching vibration of aromatic ether bonds. Both the crosslinked polymers were found to be insoluble in all common organic solvents. Consequently, they were further characterized by solid-state ^{13}C NMR to further characterize their structures **(**Fig. 1**b)**. The peaks at δ = 23.4 ppm, 48.0 ppm and 67.7 ppm can be ascribed to the methyl and methylene carbon atoms of the triptycene monomer. The carbon atom of the cyanogen exhibited a weak peak at δ = 113.8 ppm. The aromatic carbon atoms of benzene are the most abundant in the crosslinked polymers with a chemical shift at δ = 125.4 ppm. Aromatic ether groups are the most important connecting groups in the structure of the crosslinked polymeric networks and exhibit an obvious peak at δ = 143.7 ppm. In addition, the two peaks at δ = 224.6 ppm and 242.2 ppm can be attributed to the C-F bonds in the benzene rings.

Additionally, TGA analysis under a nitrogen atmosphere was performed to estimate the thermal stability of P1 and P2 (**Fig. S8**). The flow rate of N_2 was 100 mL/min and the rate of temperature decrease was 10 °C/min. The TGA curves indicate the weight losses of P1 and P2 are 8.5% and 6.6% at 400 °C, respectively. This may be attributed to the collapse of the porous polymeric network at high temperature. The char yields of P1 and P2 are 60.3% and 64.5% at 800 °C owing to the rigid triptycene and pentiptycene structures in the architecture of the porous polymers. The XRD spectra of both P1 and P2 showed broad peaks at approximately 23°, indicating these polymers are amorphous (**Fig. S9**). This can be mostly attributed to the presence of rigid triptycene and pentiptycene residues in the polymeric networks, which leads to decreased packing efficiency and relatively poor crystallinity for both P1 and P2.

In addition, the specific surface areas, average pore volumes and pore size distributions of P1 and P2 by nitrogen adsorption-desorption experiments, and the results are shown in **Fig. S10** and **Table S1**. The Brunauer-Emmett-Teller (BET) surface areas (S_{BET}) of P1 and P2 are 14.46 m^2 g^{-1} and 97.95 m^2 g^{-1}, and the pore volume are 0.029 cm^3 g^{-1} and 0.12 cm^3 g^{-1}, respectively. The pore size distribution curves reveal that the pore diameters of P1 and P2 are mainly ranging from 2 nm to 4 nm.

Furthermore, the SEM and TEM images of polymers at the same scale prove that P1 and P2 display different pore sizes (**Fig. S11 and** Fig. 2). The structure of P1 is very compact, however, the structure of P2 is relatively homogeneous and its pore sizes are suitable for the adsorption of dyes or phenolic organic pollutants. This may be the main reason for their different adsorption performances.

3.2. Dye adsorption performance

With porous structures inside the polymeric networks, the resulting crosslinking polymers possess good adsorption capacities for dyes and phenolic organic pollutants in aqueous solutions, thus both P1 and P2 can be candidates for the adsorbent materials for such organic pollutants. In order to evaluate the performance of P1 and P2 as the adsorbents for dyes, one cationic dye and one anionic dye were selected - methylene blue (MB) and methyl orange (MO), respectively. To compare the adsorption abilities towards different dye solutions (MB and MO), 15 mg of adsorbent materials each were poured into 30 mL aqueous dye solutions (10 ppm) with stirring; the UV–Vis spectra were recorded every five minutes until the adsorption equilibrium was reached. The removal efficiency was calculated according to the change in UV–vis intensity and the results are shown in Fig. 3. For methylene blue aqueous solutions, the removal efficiency of P2 reaches 99% within 40 min (nearly complete adsorption), whereas that of P1 is 96% in the same time periods. Within the initial 10 min, P2 and P1 adsorb approximately 65% and 62% of the amount of methylene blue, respectively. For aqueous

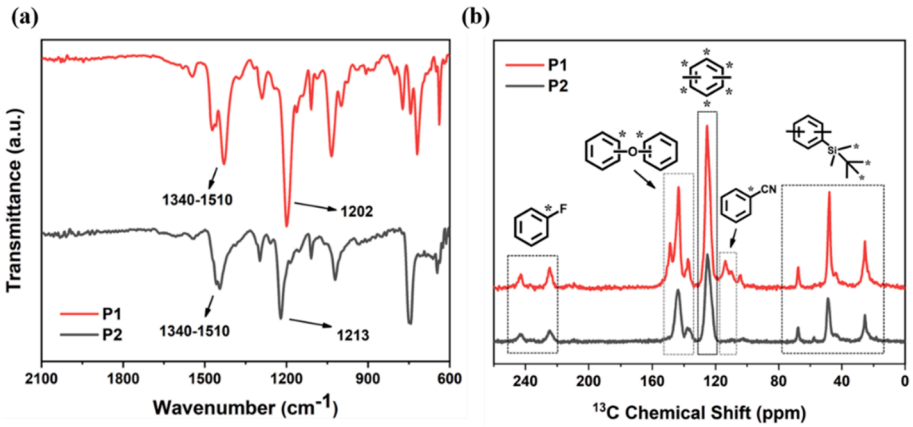

Fig. 1. (a) FT-IR spectra of and (b) solid-state ^{13}C NMR spectra of P1 and P2.

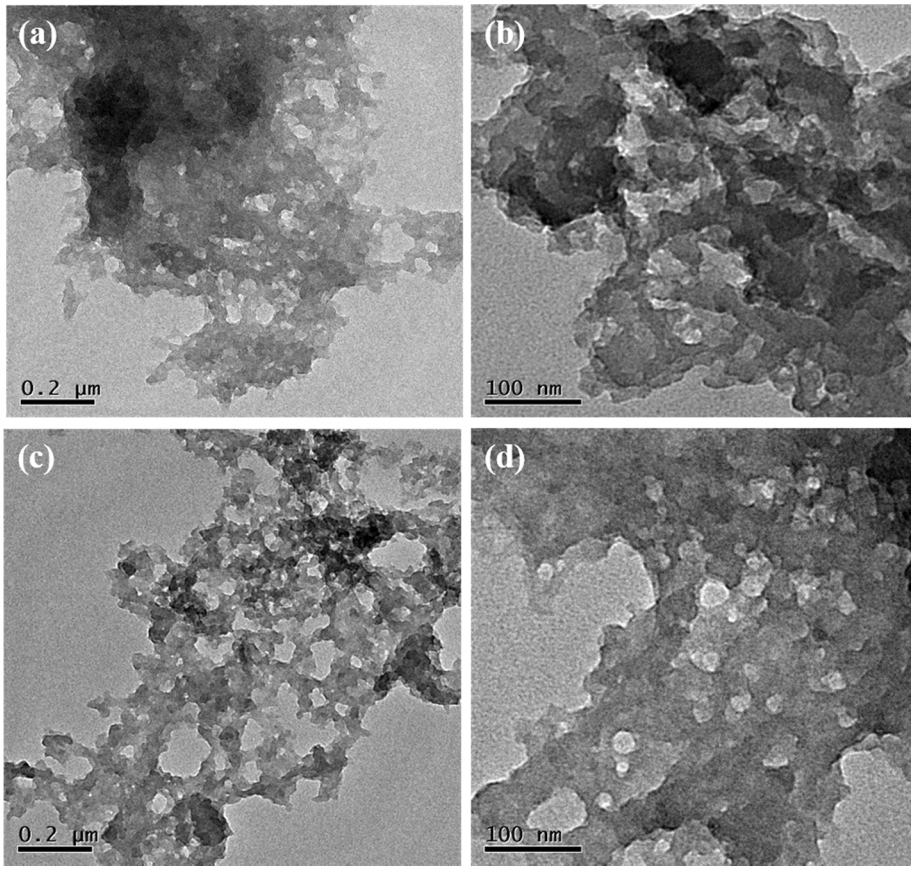

Fig. 2. TEM images of P1 (a), P2 (c) and the corresponding partial enlarged figures of P1 (b), P2 (d).

methyl orange solution, both P1 and P2 can adsorb 99% the amount of the MO solutions within 45 min. Within the initial 10 min, the removal efficiencies of P2 and P1 are 49% and 43%, respectively. The above results indicate that the adsorption speed of P2 for both cationic and anionic dyes is slightly higher than that of P1. Furthermore, the adsorption kinetics of both P1 and P2 towards MB and MO were investigated, and the results are shown in **Table. S2** and **Figs. S12–S13**. Comparing the correlation coefficient (R^2) of the pseudo-first-order and pseudo-second-order dynamic models, the R^2 of the pseudo-second-order model is higher, indicating the adsorption data is in good agreement with the pseudo-second-order kinetic model.

The q_e of the crosslinked polymers towards MB and MO were investigated and the results are shown in Table 1 **and Figs. S14–S15**. The concentrations of MB and MO used in this experiment are 10, 20, 30, 50, 100, 200 ppm, respectively. 20 mg of adsorbents were poured into 20 mL aqueous dye solutions with different concentrations and vigorously stirred for 24 h to make sure the adsorption equilibrium was reached. The q_e of adsorbents for dyes with different initial concentrations were calculated using UV–Vis spectra and the data were fitted with Langmuir model and Freundlich model. For MB, the q_e of P1 and P2 calculated from Langmuir model are 250.85 mg g^{-1}, 437.74 mg g^{-1} and the 1/n calculated from Freundlich model are 0.726, 0.824, respectively, indicating the good adsorption properties of both P1 and P2 for MB. In addition, for MO, the adsorption properties of P1 and P2 are relatively lower than those of MB. The q_e of P1 and P2 for MO calculated from Langmuir model are 150.38 mg g^{-1}, 193.43 mg g^{-1} and the 1/n

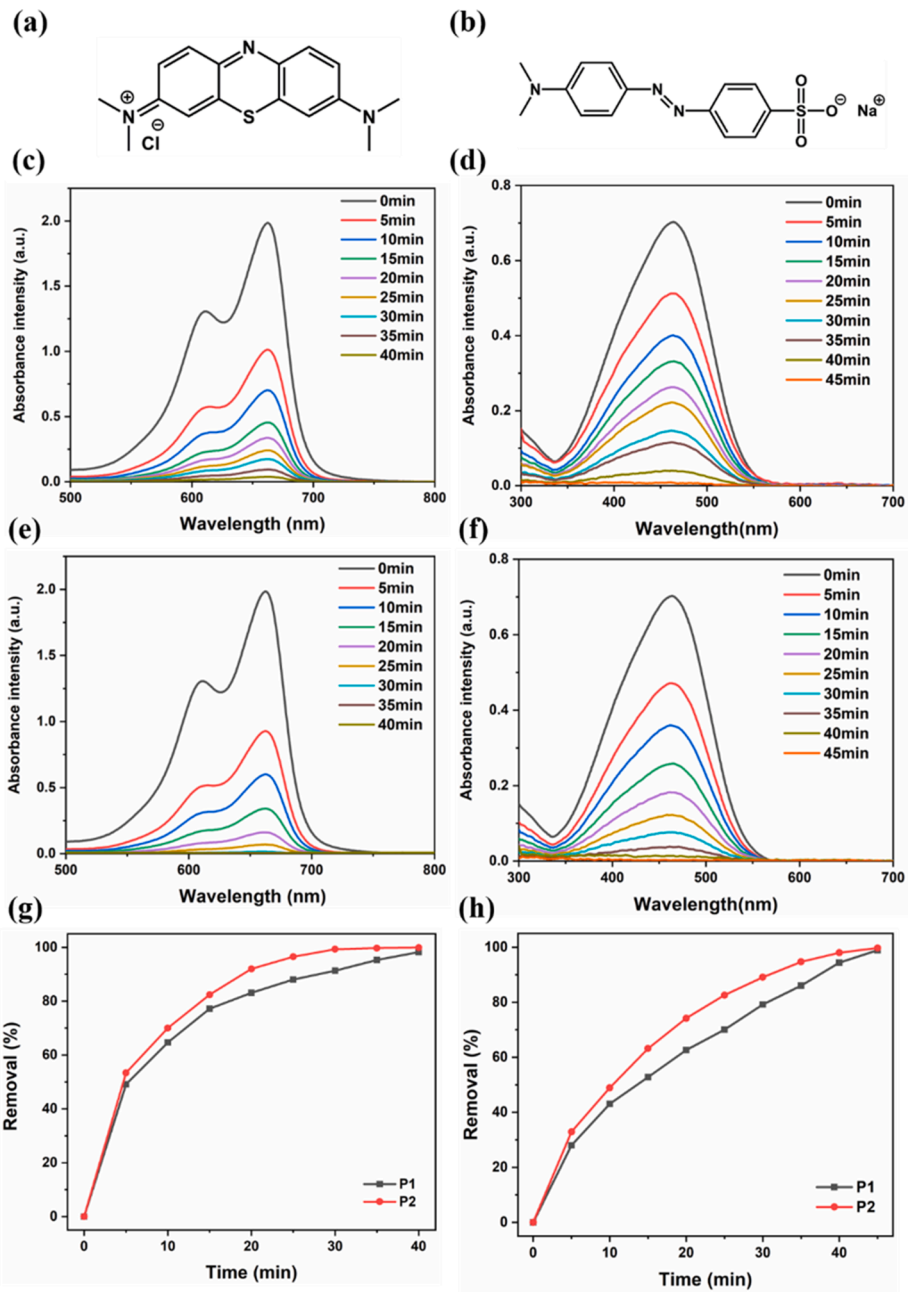

Fig. 3. Chemical structures of (a) methylene blue and (b) methyl orange. UV–vis spectra of methylene blue aqueous solution using (c) P1, (e) P2 at different time intervals and methyl orange aqueous solution using (d) P1, (f) P2 at different time intervals, the original concentrations of methylene blue and methyl orange are both 10 ppm. Time-dependent adsorption removal efficiency of (g) methylene blue and (h) methyl orange with the addition of P1 and P2. All the concentrations of the above adsorbent materials are 0.5 mg mL^{-1}. (For interpretation of the references to colour in this figure legend, the reader is referred to the web version of this article.)

Table 1
The adsorption equilibrium parameters of P1 and P2 towards MB, MO, Pol and BPA.

Pollutants	Adsorbents	Langmuir model		Freundlich model	
		q_m(mg g^{-1})	R^2	1/n	R^2
MB	P1	250.85	0.9985	0.726	0.9943
	P2	437.74	0.9927	0.824	0.9871
MO	P1	150.38	0.9877	0.653	0.9928
	P2	193.43	0.9959	0.686	0.9967
Pol	P1	38.83	0.9933	0.471	0.9465
	P2	58.73	0.9897	0.511	0.9369
BPA	P1	212.06	0.9908	0.715	0.9762
	P2	330.02	0.9945	0.776	0.9864

calculated from Freundlich model are 0.653, 0.686, respectively. In addition, the comparison of q_e of P1 and P2 towards MB and MO with some other current materials are shown in **Table S3**.

3.3. Phenolic organic pollutant adsorption performance

Compared with the adsorption performance of organic dyes, the adsorption rates of P1 and P2 for phenolic organic pollutants are much higher. Phenol (Pol) and bisphenol A (BPA) were selected as representative examples of organic phenolic pollutants for the adsorption experiments. 15 mg adsorbent materials were each poured into 30 mL phenolic organic pollutants (10 ppm) with stirring and the UV–Vis spectra were recorded every five minutes with the addition of chromogenic reagent until the adsorption equilibrium was reached. The results are displayed in Fig. 4. For phenol, the removal efficiencies of P1 and P2 are 78% and 90% at 40 min, respectively. At 5 min, P1 adsorbed 59% of the phenol, however, P2 can adsorb 89% over the same time period,

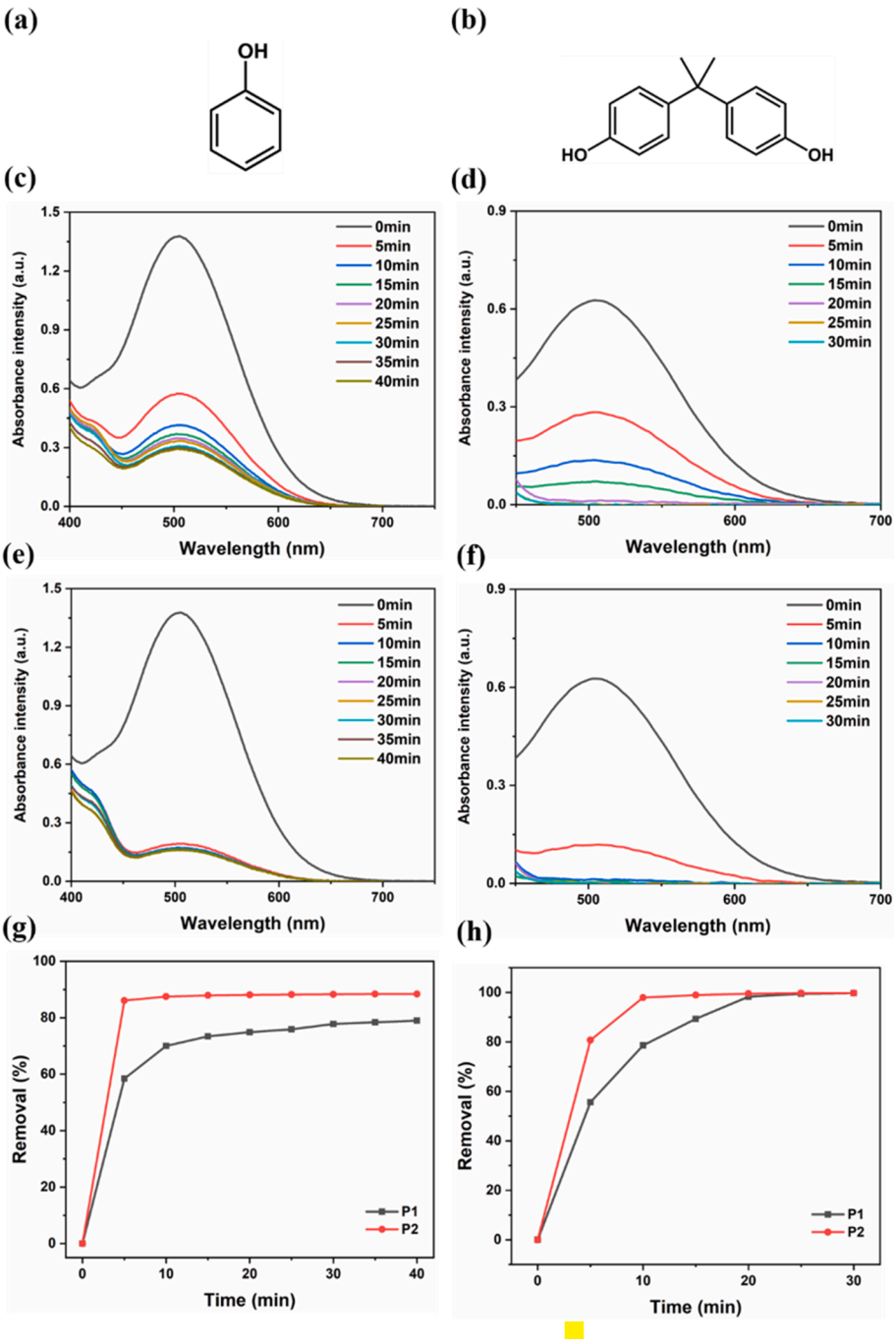

Fig. 4. Chemical structures of (a) phenol and (b) bisphenol A. UV–vis spectra of phenol aqueous solution using (c) P1, (e) P2 at different time intervals and aqueous bisphenol A solution using (d) P1 and (f) P2 at different time intervals with the addition of chromogenic reagent; the original concentrations of phenol and bisphenol A are both 10 ppm. Time-dependent adsorption removal efficiency of (g) phenol and (h) bisphenol A with the addition of P1 and P2. All the concentrations of the above adsorbent materials are 0.5 mg mL^{-1}.

almost reaching the adsorption equilibrium. For bisphenol A, P2 can reach the adsorption equilibrium within 10 min and the removal efficiency is more than 99%, approaching complete adsorption. However, the time for P1 to reach the adsorption equilibrium and removal efficiency also reaches 99%. The above results demonstrate that the adsorption speed of P2 for phenolic organic pollutants is much higher than that of P1 and more suitable for use as efficient adsorbents for phenolic organic pollutants. In order to verify the successful adsorption of bisphenol A for these two porous polymers, we compared the FT-IR spectra before and after the adsorption process (**Fig. S18**). P1 and P2 (15 mg each) were added into two bottles of aqueous bisphenol A solution (10 ppm, 30 mL) with stirring for 12 h to ensure the adsorption equilibrium is reached. Next, the mixtures were centrifuged and the solids were collected and dried at 60 °C in a vacuum overnight for the FT-IR test. Compared with the FT-IR spectra of P1 and P2, new adsorption bands in the 2800–3000 cm^{-1} region appeared, which can be attributed to the stretching vibration of the C-H bonds and methyl groups in the bisphenol A molecules. In addition, an obvious peak at 1661 cm^{-1} also appeared which can be ascribed to the vibration of the benzene ring skeleton. To a certain extent, the FI-IR spectra before and after the adsorption process could demonstrate the successful adsorption of bisphenol A using these polymeric absorbents.

Additionally, the q_e of adsorbents for phenol and BPA with different initial concentrations were performed and the data were fitted with Langmuir model and Freundlich model. The results are shown in Table. 1 and **Figs. S16–S17**. For Pol, the saturated adsorption capacities of P1 and P2 calculated from Langmuir model are 38.83 mg g^{-1}, 58.73 mg g^{-1} and the 1/n calculated from Freundlich model are 0.471, 0.511,

respectively. However, for BPA, the adsorption properties of P1 and P2 are much better. The saturated adsorption capacities of P1 and P2 for BPA calculated from Langmuir model are 212.06 mg g^{-1}, 330.02 mg g^{-1} and the 1/n calculated from Freundlich model are 0.715, 0.776, respectively. In addition, the comparison of q_e of P1 and P2 towards BPA with some other current materials are shown in **Table S4**.

3.4. Removal efficiency of different organic pollutants

We further studied the adsorption selectivity of P1 and P2 for phenolic organic pollutants (Fig. 5). The removal efficiency of P1 and P2 towards various common phenolic organic pollutants including 2,4,6-tribromophenol, bis(4-hydroxyphenyl) sulfone, bisphenol A, 4-nitrophenol, 2-naphthol, p-cresol and phenol were investigated. In addition, the removal efficiencies of P1 and P2 for non-hydroxyl aromatic pollutants such as toluene, chlorobenzene and alcohols, including methanol and ethanol, were also performed. The original concentrations of all the above organic pollutants were 10 ppm at 25 °C. Next, all the above aqueous solutions of the organic pollutants were stirred with adsorbents overnight to allow the adsorption equilibrium to be reached. The results are displayed in Fig. 5. In general, the trends in removal efficiency for both P1 and P2 towards various organic pollutants with different structures are the same. The removal efficiencies of both P1 and P2 for 2,4,6-tribromophenol (TBP), bis(4-hydroxyphenyl) sulfone (BPS), bisphenol A (BPA) and 4-nitrophenol (NP), 2-naphthol (NPT) are >99%, approaching complete adsorption. In addition, the removal efficiencies of P1 for p-methylphenol (MP) and phenol (Pol) are 95.7% and 78.5%, and those of P2 are 90.1% and 90.3%, respectively. However, P1 and P2 are not suitable adsorbents for aromatic organic pollutants, which do not contain hydroxyl groups, and common alcohols. Toluene (Tol), chlorobenzene (CB) methanol (Mol) and ethanol (Eol) are representative compounds. Only 1%-2% of Tol, CB, Mol and Eol can be adsorbed by P1 and P2. The selective adsorption of P1 and P2 towards phenolic organic pollutants can most likely be attributed to two factors: 1) The formation of intermolecular hydrogen bonds between the fluorine atoms of the crosslinked polymers and phenolic hydroxyl groups increases the affinity of adsorbents towards phenolic organic pollutants; 2) The pore sizes of P1 and P2 may be suitable for the adsorption of phenolic organic compounds, rather than non-alcoholic aromatic pollutants or other alcohols [35,45]. Consequently, the above results indicate that P1 and P2 are good adsorbents for phenolic organic pollutants.

3.5. Recycling experiments

The recycling experiments of both P1 and P2 for the BPA removal were performed to test the stability of the adsorbents. (Fig. 6) P1 or P2 (both 10 mg) was added to a solution of BPA (20 mL, 10 ppm) in distilled water. After stirring for 12 h, an adsorption equilibrium was reached and the removal efficiency of BPA was calculated according to the change in UV–vis adsorption intensity. The mixture was centrifuged and the obtained adsorbent materials were soaked in ethanol for 6 h. An additional centrifugation was carried out and the obtained adsorbent materials were successively washed with distilled water and ethanol, and then dried at 80 °C under vacuum to give a scarlet solid which could be used in the next cyclic test. In the cyclic adsorption experiment, the removal efficiency of P1 decreased from 99.4% to 98.5% and P2 decreased from 99.5% to 98.3% after five adsorption cycles, and 81.4% and 84.6% after 15 cycles, confirming the stability of the adsorbent materials. In addition, the reason for the reduction in removal efficiency could be mainly attributed to the minor weight loss of adsorbent material during the centrifugation and washing process.

4. Conclusion

In summary, two triptycene- and pentiptycene-based functional monomers were polymerized using TFTP as the crosslinker in order to prepare two highly crosslinked polymers named P1 and P2. The reaction is simple and can be conducted at a relatively mild temperature. Both P1 and P2 display fast and efficient adsorption capacities for dyes and phenolic organic pollutants with low concentrations in aqueous solutions. The removal efficiency of P2 can reach >99% within 10 min for bisphenol A. Additionally, the adsorption kinetics and isotherms are more suitable for the pseudo-second-order and Langmuir models, respectively. The maximum adsorption capacities of P1 and P2 for BPA are as high as 212.06 and 330.02 mg g^{-1}. More importantly, they show almost no adsorption for non-alcoholic aromatic organic pollutants and common alcohols, indicating their highly selective adsorption abilities for phenolic organic pollutants. Furthermore, the removal efficiencies of both P1 and P2 for bisphenol A remain nearly constant after five cycles. Due to their simple synthesis, porous architecture and efficient adsorption capability, such triptycene- and pentiptycene-based crosslinked polymers may be versatile adsorbent materials for application in water treatment and purification.

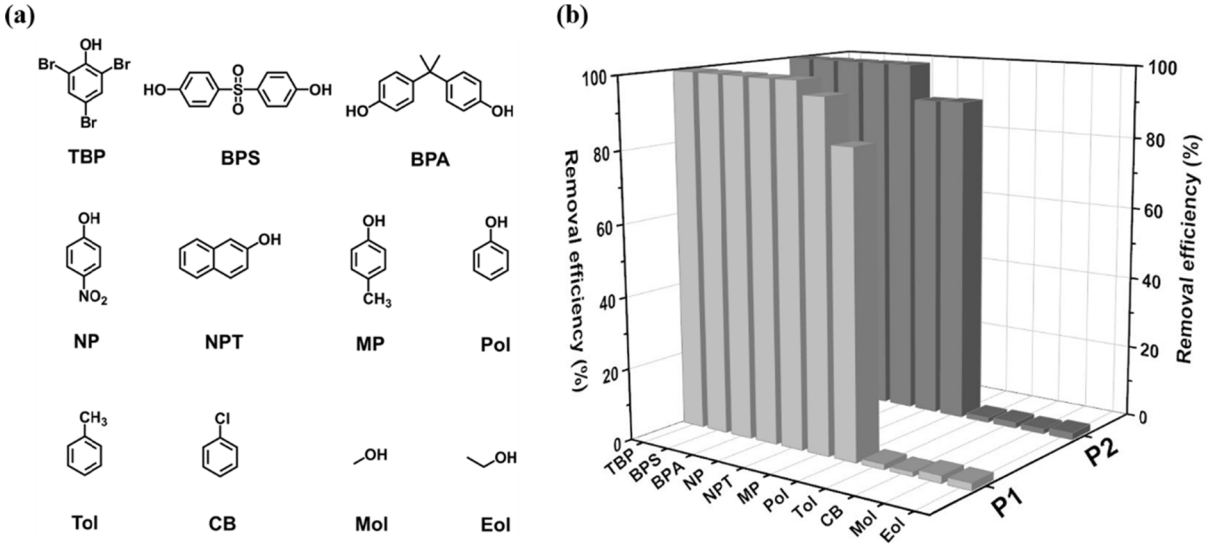

Fig. 5. (a) The chemical structures of the different organic pollutants used for the adsorption experiment. (b) Removal efficiencies of P1 and P2 for various organic pollutants.

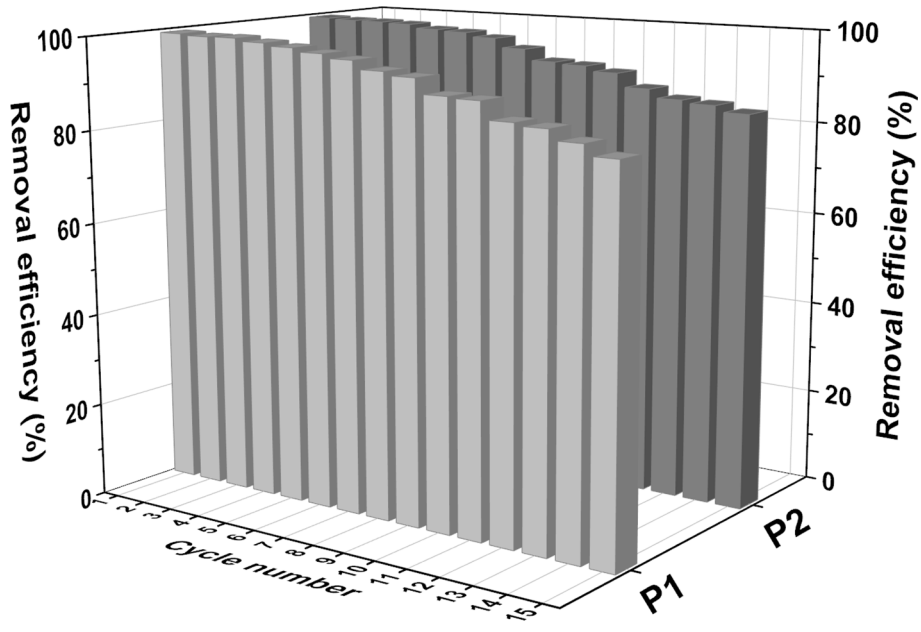

Fig. 6. Reusability of P1 and P2 for BPA aqueous solution (10 ppm) after 15 cycles.

Declaration of Competing Interest

The authors declare that they have no known competing financial interests or personal relationships that could have appeared to influence the work reported in this paper.

Acknowledgements

We sincerely acknowledge financial support from the National Natural Science Foundation of China (51773144, 21938006, 51803143), Science Foundation of Jiangsu Province (BE2019659), the NSF of the Jiangsu Province Higher Education Institutions of China (20KJA610001) and PAPD in Jiangsu Province and Science Foundation of Suzhou City (SS2019025).

We greatly acknowledge the Priority Academic Program Development of Higher Education Institutions (PAPD) in Jiangsu and National Center for International Research on Intelligent Nano Materials and Detection Technology in Environmental Protection for their support.

Appendix A. Supplementary material

Supplementary data to this article can be found online at https://doi.org/10.1016/j.seppur.2021.119495.

References

[1] S.D. Richardson, S.Y. Kimura, Water Analysis: Emerging Contaminants and Current Issues, Anal. Chem. 88 (2016) 546–582.
[2] B. Petrie, R. Barden, B. Kasprzyk-Hordern, A review on emerging contaminants in wastewaters and the environment: current knowledge, understudied areas and recommendations for future monitoring, Water Res. 72 (2015) 3–27.
[3] O. Rozas, C. Vidal, C. Baeza, W.F. Jardim, A. Rossner, H.D. Mansilla, Organic micropollutants (OMPs) in natural waters: Oxidation by UV/H2O2 treatment and toxicity assessment, Water Res. 98 (2016) 109–118.
[4] K. Choi, Y. Kim, J. Park, C.K. Park, M. Kim, H.S. Kim, P. Kim, Seasonal variations of several pharmaceutical residues in surface water and sewage treatment plants of Han River, Korea, Sci. Total Environ. 405 (2008) 120–128.
[5] K.E. Murray, S.M. Thomas, A.A. Bodour, Prioritizing research for trace pollutants and emerging contaminants in the freshwater environment, Environ. Pollut. 158 (2010) 3462–3471.
[6] R. McKinlay, J.A. Plant, J.N. Bell, N. Voulvoulis, Calculating human exposure to endocrine disrupting pesticides via agricultural and non-agricultural exposure routes, Sci. Total Environ. 398 (2008) 1–12.
[7] S. Zheng, J. Shi, J. Zhang, Y. Yang, J. Hu, B. Shao, Identification of the disinfection byproducts of bisphenol S and the disrupting effect on peroxisome proliferator-activated receptor gamma (PPARgamma) induced by chlorination, Water Res. 132 (2018) 167–176.
[8] D. Wu, L. He, R. Sun, M. Tong, H. Kim, Influence of Bisphenol A on the transport and deposition behaviors of bacteria in quartz sand, Water Res. 121 (2017) 1–10.
[9] B. Liu, H.-J. Lehmler, Y. Sun, G. Xu, Y. Liu, G. Zong, Q. Sun, F.B. Hu, R.B. Wallace, W. Bao, Bisphenol A substitutes and obesity in US adults: analysis of a population-based, cross-sectional study, Lancet Planetary Health 1 (2017) e114–e122.
[10] Y. Li, P. Lu, J. Cheng, X. Zhu, W. Guo, L. Liu, Q. Wang, C. He, S. Liu, Novel microporous beta-cyclodextrin polymer as sorbent for solid-phase extraction of bisphenols in water samples and orange juice, Talanta 187 (2018) 207–215.
[11] C. Palomino Cabello, M.F.F. Picó, F. Maya, M. del Rio, G. Turnes Palomino, UiO-66 derived etched carbon/polymer membranes: High-performance supports for the extraction of organic pollutants from water, Chem. Eng. J. 346 (2018) 85–93.
[12] S. Karak, K. Dey, A. Torris, A. Halder, S. Bera, F. Kanheerampockil, R. Banerjee, Inducing Disorder in Order: Hierarchically Porous Covalent Organic Framework Nanostructures for Rapid Removal of Persistent Organic Pollutants, J. Am. Chem. Soc. 141 (2019) 7572–7581.
[13] R. Zhao, Y. Tian, S. Li, T. Ma, H. Lei, G. Zhu, An electrospun fiber based metal–organic framework composite membrane for fast, continuous, and simultaneous removal of insoluble and soluble contaminants from water, J. Mater. Chem. A 7 (2019) 22559–22570.
[14] R. Ji, J. Liu, T. Zhang, Y. Peng, Y. Li, D. Chen, Q. Xu, J. Lu, Construction of a ternary Z-scheme In2S3@Au@P3HT photocatalyst for the degradation of phenolic pollutants under visible light, Sep. Purif. Technol. 272 (2021).
[15] J. Liu, S. Zhou, P. Gu, T. Zhang, D. Chen, N. Li, Q. Xu, J. Lu, Conjugate Polymer-clothed TiO2@V2O5 nanobelts and their enhanced visible light photocatalytic performance in water remediation, J. Colloid Interface Sci. 578 (2020) 402–411.
[16] A. Alsbaiee, B.J. Smith, L. Xiao, Y. Ling, D.E. Helbling, W.R. Dichtel, Rapid removal of organic micropollutants from water by a porous beta-cyclodextrin polymer, Nature 529 (2016) 190–194.
[17] M.A. Shannon, P.W. Bohn, M. Elimelech, J.G. Georgiadis, B.J. Marinas, A. M. Mayes, Science and technology for water purification in the coming decades, Nature 452 (2008) 301–310.
[18] M.-L. Liu, L. Li, Y.-X. Sun, Z.-J. Fu, X.-L. Cao, S.-P. Sun, Scalable conductive polymer membranes for ultrafast organic pollutants removal, J. Membr. Sci. 617 (2021).
[19] W. Ren, J. Gao, C. Lei, Y. Xie, Y. Cai, Q. Ni, J. Yao, Recyclable metal-organic framework/cellulose aerogels for activating peroxymonosulfate to degrade organic pollutants, Chem. Eng. J. 349 (2018) 766–774.
[20] C. Li, H. Xu, J. Gao, W. Du, L. Shangguan, X. Zhang, R.-B. Lin, H. Wu, W. Zhou, X. Liu, J. Yao, B. Chen, Tunable titanium metal–organic frameworks with infinite 1D Ti–O rods for efficient visible-light-driven photocatalytic H2 evolution, J. Mater. Chem. A 7 (2019) 11928–11933.
[21] L. Wang, H. Xu, J. Gao, J. Yao, Q. Zhang, Recent progress in metal-organic frameworks-based hydrogels and aerogels and their applications, Coord. Chem. Rev. 398 (2019).
[22] T. Skorjanc, D. Shetty, S.K. Sharma, J. Raya, H. Traboulsi, D.S. Han, J. Lalla, R. Newlon, R. Jagannathan, S. Kirmizialtin, J.C. Olsen, A. Trabolsi, Redox-Responsive Covalent Organic Nanosheets from Viologens and Calix[4]arene for Iodine and Toxic Dye Capture, Eur. Polym. J. 24 (2018) 8648–8655.
[23] X. Li, M. Zhou, J. Jia, J. Ma, Q. Jia, Design of a hyper-crosslinked β-cyclodextrin porous polymer for highly efficient removal toward bisphenol a from water, Sep. Purif. Technol. 195 (2018) 130–137.

[24] L. Xiao, Y. Ling, A. Alsbaiee, C. Li, D.E. Helbling, W.R. Dichtel, beta-Cyclodextrin Polymer Network Sequesters Perfluorooctanoic Acid at Environmentally Relevant Concentrations, J. Am. Chem. Soc. 139 (2017) 7689–7692.
[25] Z. Yang, Y. Gu, B. Yuan, Y. Tian, J. Shang, D.C.W. Tsang, M. Liu, L. Gan, S. Mao, L. Li, Thio-groups decorated covalent triazine frameworks for selective mercury removal, J. Hazard. Mater. 403 (2021), 123702.
[26] X. Tang, G. Ran, J. Li, Z. Zhang, C. Xiang, Extremely efficient and rapidly adsorb methylene blue using porous adsorbent prepared from waste paper: Kinetics and equilibrium studies, J. Hazard. Mater. 402 (2021), 123579.
[27] J. Fan, A. Li, W. Yang, L. Yang, Q. Zhang, Adsorption of water-soluble dye X-BR onto styrene and acrylic ester resins, Sep. Purif. Technol. 51 (2006) 338–344.
[28] N. Jiang, R. Shang, S.G.J. Heijman, L.C. Rietveld, Adsorption of triclosan, trichlorophenol and phenol by high-silica zeolites: Adsorption efficiencies and mechanisms, Sep. Purif. Technol. 235 (2020).
[29] L.P. Skala, A. Yang, M.J. Klemes, L. Xiao, W.R. Dichtel, Resorcinarene Cavitand Polymers for the Remediation of Halomethanes and 1,4-Dioxane, J. Am. Chem. Soc. 141 (2019) 13315–13319.
[30] X. Suo, Y. Yu, S. Qian, L. Zhou, X. Cui, H. Xing, Tailoring the Pore Size and Chemistry of Ionic Ultramicroporous Polymers for Trace Sulfur Dioxide Capture with High Capacity and Selectivity, Angew. Chem. Int. Ed. Engl. 60 (2021) 6986–6991.
[31] J. Jia, Z. Chen, H. Jiang, Y. Belmabkhout, G. Mouchaham, H. Aggarwal, K. Adil, E. Abou-Hamad, J. Czaban-Jóźwiak, M.R. Tchalala, M. Eddaoudi, Extremely Hydrophobic POPs to Access Highly Porous Storage Media and Capturing Agent for Organic Vapors, Chem 5 (2019) 180–191.
[32] K. Jie, Y. Zhou, Q. Sun, B. Li, R. Zhao, D.-E. Jiang, W. Guo, H. Chen, Z. Yang, F. Huang, S. Dai, Mechanochemical synthesis of pillar[5]quinone derived multi-microporous organic polymers for radioactive organic iodide capture and storage, Nat. Commun. 11 (2020).
[33] J. Wu, F. Xu, S. Li, P. Ma, X. Zhang, Q. Liu, R. Fu, D. Wu, Porous Polymers as Multifunctional Material Platforms toward Task-Specific Applications, Adv. Mater. 31 (2019), e1802922.
[34] Q. Chen, A. Dong, D. Wang, L. Qiu, C. Ma, Y. Yuan, Y. Zhao, N. Jia, Z. Guo, N. Wang, Efficient and Selective Methane Borylation Through Pore Size Tuning of Hybrid Porous Organic-Polymer-Based Iridium Catalysts, Angew. Chem. Int. Ed. Engl. 58 (2019) 10671–10676.
[35] D. Shetty, I. Jahovic, J. Raya, Z. Asfari, J.C. Olsen, A. Trabolsi, Porous Polycalix[4]arenes for Fast and Efficient Removal of Organic Micropollutants from Water, ACS Appl. Mater. Interfaces 10 (2018) 2976–2981.
[36] O. Buyukcakir, Y. Seo, A. Coskun, Thinking Outside the Cage: Controlling the Extrinsic Porosity and Gas Uptake Properties of Shape-Persistent Molecular Cages in Nanoporous Polymers, Chem. Mater. 27 (2015) 4149–4155.
[37] A.K. Sekizkardes, T. İslamoğlu, Z. Kahveci, H.M. El-Kaderi, Application of pyrene-derived benzimidazole-linked polymers to CO2 separation under pressure and vacuum swing adsorption settings, J. Mater. Chem. A 2 (2014) 12492–12500.
[38] W. Bai, Y. Fan, F. Wang, P. Mu, H. Sun, Z. Zhu, W. Liang, A. Li, Facile synthesis of porous organic polymers (POPs) membrane via click chemistry for efficient PM2.5 capture, Sep. Purifi. Technol. 258 (2021).
[39] D. Dai, J. Yang, Y.C. Zou, J.R. Wu, L.L. Tan, Y. Wang, B. Li, T. Lu, B. Wang, Y. W. Yang, Macrocyclic Arenes-Based Conjugated Macrocycle Polymers for Highly Selective CO2 Capture and Iodine Adsorption, Angew. Chem. Int. Ed. Engl. 60 (2021) 8967–8975.
[40] X. Wang, L. Xie, K. Lin, W. Ma, T. Zhao, X. Ji, M. Alyami, N.M. Khashab, H. Wang, J.L. Sessler, Calix[4]pyrrole-Crosslinked Porous Polymeric Networks for the Removal of Micropollutants from Water, Angew. Chem. Int. Ed. Engl. 60 (2021) 7188–7196.
[41] Z. Jia, J. Pan, C. Tian, D. Yuan, Twisted molecule-based hyper-crosslinked porous polymers for rapid and efficient removal of organic micropollutants from water, RSC Adv. 8 (2018) 36812–36818.
[42] S. Luo, Q. Zhang, Y. Zhang, K.P. Weaver, W.A. Phillip, R. Guo, Facile Synthesis of a Pentiptycene-Based Highly Microporous Organic Polymer for Gas Storage and Water Treatment, ACS Appl. Mater. Interfaces 10 (2018) 15174–15182.
[43] C. Zhang, P.-C. Zhu, L. Tan, J.-M. Liu, B. Tan, X.-L. Yang, H.-B. Xu, Triptycene-Based Hyper-Cross-Linked Polymer Sponge for Gas Storage and Water Treatment, Macromolecules 48 (2015) 8509–8514.
[44] R. Bera, M. Ansari, S. Mondal, N. Das, Selective CO2 capture and versatile dye adsorption using a microporous polymer with triptycene and 1,2,3-triazole motifs, Eur. Polym. J. 99 (2018) 259–267.
[45] Z. Wang, F. Cui, Y. Pan, L. Hou, B. Zhang, Y. Li, L. Zhu, Hierarchically micro-mesoporous beta-cyclodextrin polymers used for ultrafast removal of micropollutants from water, Carbohydr. Polym. 213 (2019) 352–360.